Different Methods of Increasing the Mechanical Strength of Gold Nanocages

ARTICLE *in* JOURNAL OF PHYSICAL CHEMISTRY LETTERS · NOVEMBER 2012

Impact Factor: 7.46 · DOI: 10.1021/jz301503z

3 AUTHORS, INCLUDING:

Mahmoud A. Mahmoud
Georgia Institute of Technology
76 PUBLICATIONS **1,806** CITATIONS
SEE PROFILE

Mostafa A El-Sayed
Georgia Institute of Technology
676 PUBLICATIONS **54,961** CITATIONS
SEE PROFILE

THE JOURNAL OF PHYSICAL CHEMISTRY Letters

Letter

pubs.acs.org/JPCL

Different Methods of Increasing the Mechanical Strength of Gold Nanocages

Mahmoud A. Mahmoud, Paul Szymanski, and Mostafa A. El-Sayed*

Laser Dynamics Laboratory, School of Chemistry and Biochemistry, Georgia Institute of Technology, Atlanta, Georgia 30332-0400, United States

Supporting Information

ABSTRACT: Using the ultrafast coherent modulation of the surface plasmon band intensity with the totally symmetric lattice vibration of gold nanocages, we were able to determine and use their frequencies as a measure of the cage's mechanical stability. The presence of an inner "stiff" transition-metal nanoshell with a higher value of the elastic modulus is found to increase the frequency of the lattice vibration of the outer soft gold nanoshell. This could also explain the observed increase in both the gold lattice vibrational frequency as well as the lattice vibration relaxation time in the Au–Pt and Au–Pd double-shell nanocages. It is also found that when these nanoparticles are assembled into monolayers on quartz substrates by the Langmuir–Blodgett technique, the oscillation frequency of the gold shell with the transition metal having the largest elastic constant suffers the least change in its oscillation frequency as a result of its resistance to distortion as a result of binding to the substrate.

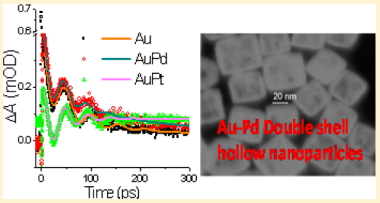

SECTION: Physical Processes in Nanomaterials and Nanostructures

Plasmonic noble-metal nanostructures attract much interest because of their unique optical,[1−3] photothermal, photoelectromagnetic,[4] and photoacoustic[5] properties, which result from their large scattering and absorption cross sections due to their localized surface plasmon resonances (LSPRs).[1−3] The above properties are tunable by changing the shape, size, and the dielectric function of the medium and the composition of the nanoparticle. Different shapes have been prepared such as spheres,[6] cubes,[7−9] nanocages,[7,8] rods,[10,11] stars,[12] triangles,[13] shells,[14] rings,[15] and frames[16,17] having LSPR spectra that cover the visible and near-IR regions.

Gold nanocages have many useful optical,[1−3] sensing,[18] photothermal,[19] and catalytic properties.[20,21] As hollow nanoparticles, their mechanical stability is an important factor in determining their practical usefulness for future applications. The changes in the vibrational motions of nanoparticles can be used to follow the changes in their mechanical stability.

The vibrational motions of metal nanoparticles cause periodic instantaneous changes in size and/or shape, which modulate the wavelength of the LSPR band.[22,23] Thus, the intensity of this band at a specific wavelength is modulated at a frequency corresponding to the lattice vibrational frequency of the nanoparticle. Totally symmetric vibrations of the lattice usually give the largest modulation of the electronic volume of the plasmonic nanoparticle and thus the largest modulation of the wavelength of the surface plasmon spectrum. This makes it possible to determine the symmetric lattice vibrations of plasmonic nanostructures in the optical region.[24,25] These measurements have been carried out on a wide variety of nanostructures in both ensemble[9,15,24−33] and single-particle[26,34−39] studies.

The dependence of the nanoparticle vibrational frequencies and the damping and dephasing of vibrational excitation on the nanoparticle composition and shape serve as important fundamental probes of the mechanical properties on the nanoscale.[26,28,31,32,40−42] Recently, a study has been published on Au nanorods coated with Pd.[32] A change in the mean elastic properties and particle size compared to those of uncoated nanorods affected the rod's vibrational frequency.[32] An experimental and theoretical study has been published[31] comparing Au nanocages with Au–Ag nanoboxes, with both at multiple sizes. It was concluded that the elastic constants of metals do not change on the nanoscale.[31]

Recently, we have synthesized hollow double-shell nanoparticles made of two different metals in contact.[21,43,44] On the basis of the Au nanocage structure, an inner shell of Pt or Pd is formed, while the outer shell remains Au. In the present work, we present the results of studying the modulation of the gold plasmonic band intensity at a specific wavelength to determine the perturbation of the lattice vibrational frequency of the outer gold nanoshell by the stiffer inner Pt or Pd nanoshell. Our previously observed[21,43,44] high-resolution TEM and STEM coupled to X-ray energy dispersive microanalysis images showed that alloying processes have occurred between the two shells at their joint interfaces. We found that the outer gold lattice oscillation increases in frequency in proportion to the elastic constant of the transition metal inside of the nanoshell. Inner shells result in increasing the symmetric breathing lattice vibrational frequency of the outer soft gold nanoshell. In

Received: September 24, 2012
Accepted: November 15, 2012
Published: November 15, 2012

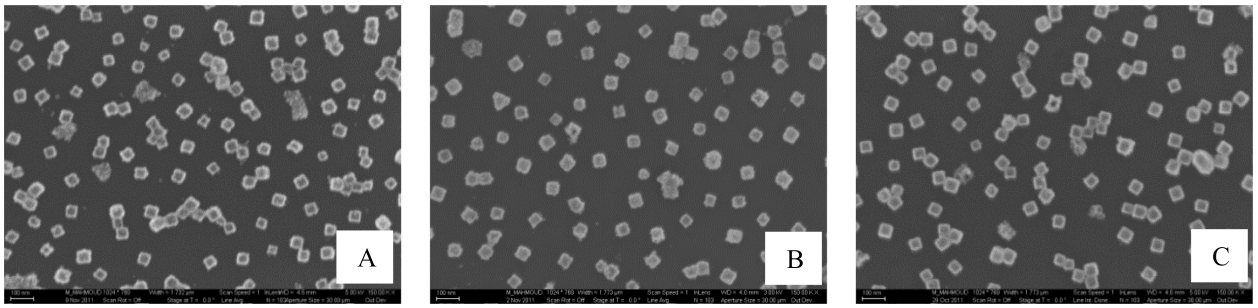

Figure 1. SEM images of (A) AuNCs, (B) AuPdNCs shell−shell, and (C) AuPtNCs shell−shell assembled on the surface of a silicon wafer at percent of coverages of 23, 24, and 23%, respectively. The scale bar in the three images is 100 nm.

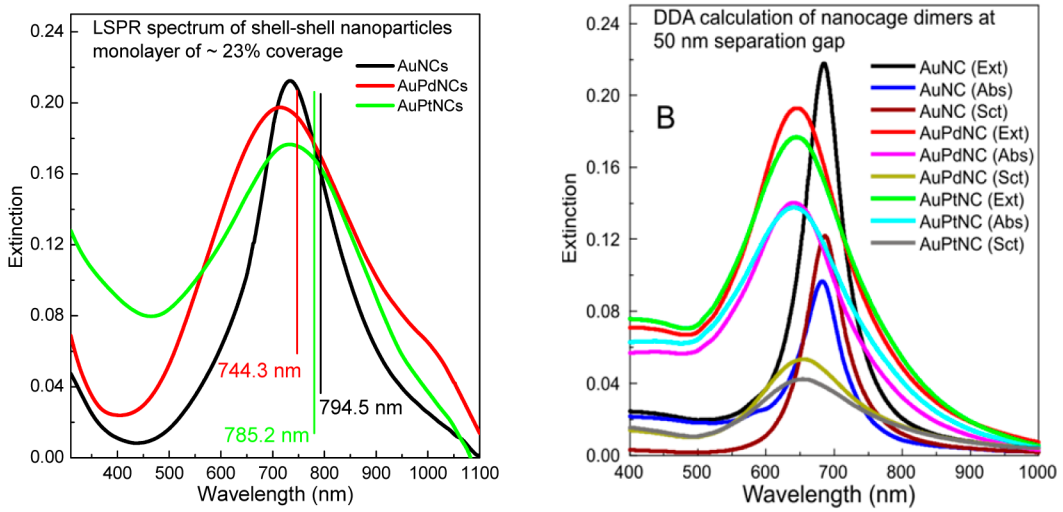

Figure 2. (A) LSPR of AuNCs, AuPdNCs, and AuPtNCs assembled on the surface of a quartz substrate at a surface density of 23%. The vertical lines show the probing wavelengths in which the dynamic oscillations results are shown in Figure 3. (B) The LSPR extinction (Ext), scattering (Sct), and absorption (Abs) of AuNCs, AuPdNCs, and AuPtNCs calculated by DDA simulation, showing that absorption dominates the extinction spectrum, which is important in carrying out the optical determination of the lattice oscillation frequency.

addition, high-resolution TEM images of the double nanocages suggest the occurrence of alloying processes at the gold−transition metal interfaces. This can also contribute to the observed increase in the gold lattice vibrational frequency in the Au−Pt and Au−Pd double-shell nanocages (see Table 1). We also observed increased vibrational frequencies when the hollow nanocages were deposited onto solid substrates or replaced with completely solid nanocubes of comparable size. These strategies can as much as double the oscillation frequency of a photoexcited plasmonic nanoparticle.

Hollow gold nanocages (AuNCs) and double-shell nanocages with an outer gold shell and an inner shell of platinum (AuPtNCs) or palladium (AuPdNCs) were prepared, as reported earlier.[21,43] Briefly, silver nanocubes (AgNCs) were used as a template for the galvanic replacement of Ag by Au,[7] Pt,[21] and Pd.[21] The as-prepared AuNCs, AuPtNCs, and AuPdNCs possessed LSPR peak maxima at 830 nm and were purified by centrifugation at 10 000 rpm for 5 min.[21,43,44] All nanoparticles were water-soluble for the solution measurements. Langmuir−Blodgett monolayers were prepared as previously reported.[17] Samples of ∼23% surface coverage were used in our measurements. A Zeiss Ultra60 was used for the scanning electron microscopy (SEM) imaging. Figure 1A−C shows the SEM images of AuNC, double-shell AuPdNC, and double-shell AuPtNC nanoparticles assembled into monolayers at coverage densities of 23, 24, and 23%, respectively, on the surfaces of silicon substrates. Image J software was used to calculate the percent of area of the substrate covered by the nanoparticles as well as the particle size and distribution, which were found to be 61 ± 4 nm for the three different nanoparticles.

Transient absorption (TA) measurements were performed with a Coherent Libra-HE regenerative-amplified Ti:sapphire laser system, which produces sub-50 fs pulses with 3.5 mJ of energy at a 1 kHz repetition rate. Approximately 5% of the 800 nm fundamental was directed into an Ultrafast Systems Helios TA spectrometer with a 3.3 ns delay range and 6.7 fs temporal scanning resolution. Supercontinuum generation was used to produce broad-band light by focusing the 800 nm beam into sapphire for probing from 450 to 820 nm or CaF_2 for probing from 350 to 750 nm. The CaF_2 crystal was continuously translated at a rate of 0.1 mm/s to prevent thermal instability. Roughly 25% of the fundamental was frequency-doubled in a BBO crystal then band-pass-filtered to produce the 400 nm pump beam. The two beams were spatially overlapped and focused onto the sample to a $1/e^2$ radius of 870 ± 20 μm (320 ± 10 μm) for the pump (probe). Aqueous solutions of nanoparticles were measured in cuvettes of optical crown glass and stirred continuously, while samples on substrates were continuously translated at a rate of 125 μm/s during the measurement. A fiber optic Si array detector was used to measure the transmitted probe spectrum with every other

dx.doi.org/10.1021/jz301503z | J. Phys. Chem. Lett. 2012, 3, 3527−3531

pump pulse blocked by an optical chopper to calculate the differential absorption ΔA as a function of the delay time t between the pump and probe. Delay times were measured in random order. The Surface Xplorer software (Ultrafast Systems) was used to extract $\Delta A(t)$ at selected wavelengths after smoothing the transient spectra.

To describe dynamics much longer than the pulse width, the TA signal at probe wavelength λ was empirically modeled as

$$A(\lambda, t) = c(\lambda) + A_1(\lambda)\cos(2\pi f_1(\lambda)t + \varphi_1(\lambda))e^{-t/\tau_1(\lambda)} + \sum_{n=2}^{3} A_n(\lambda)e^{-t/\tau_n(\lambda)} \quad (1)$$

where the A_n, τ_n, f_n, and φ_n represent the amplitudes, lifetimes, oscillation frequencies, and phases of signal components, respectively, and c is time-independent. Fits at multiple wavelengths were performed in OriginPro (Originlab Corp.) to obtain values for the parameters.

Incident pump fluences used were 8.4 μJ/cm^2 for AuNCs and AgNCs and 25 μJ/cm^2 for AuPdNCs and AuPtNCs. The same fluences were used whether the samples were in solution or on substrates. Damage thresholds of 10 mJ/cm^2 have been reported for AuNCs in aqueous solution.[30] However, we observed damage at fluences as low as 17 μJ/cm^2 on quartz substrates. Working at a fluence that gives stable signals for tens of hours of irradiation for AuNCs, even on a substrate, gives barely measurable signals for bimetallic nanocages. Differences in excitation fluence may affect the vibrational frequency when comparing different types of nanoparticles, but the measurements are not expected to be very sensitive to differences of ~20 μJ/cm^2 when working far from the solution-phase damage threshold.[30]

Figure 2A shows the LSPR spectra of AuNC, AuPdNC, and AuPtNC nanoparticles assembled into monolayers on the surfaces of quartz substrates at coverage densities of 23, 24, and 23%, respectively. The LSPR peak of AuNCs is narrow and symmetrical and is centered at 740 nm. With the addition of an interior shell of palladium or platinum, the shape of the LSPR peak becomes broader and asymmetric. The LSPR absorption and scattering as well as the interband transitions for the plasmonic nanoparticles depend on how the oscillating electrons lose their coherence. Absorption results from the electron and hole generation in the conduction band of the nanoparticle. The interband transition absorption results from the electron and hole generation in the conduction band and d band, respectively. The LSPR scattering spectrum results from emitting photons of energy similar to that of the incident photons. In order to observe the lattice oscillation, the observed extinction peaks should be largely the result of absorption and not dominated by scattering processes. In order to check on this important point, we carried out discrete dipole approximation (DDA) calculations. For direct comparison with the experimental results, the surrounding medium is air and a quartz substrate are included in the model. Figure 2B shows the calculated extinction spectra and their separation into absorption and scattering components for AuNCs, AuPdNCs, and AuPtNCs. Similar to the experimental results, the LSPR extinction peak of AuNCs is narrower than that of AuPdNCs and AuPtNCs; all simulated spectra are narrower than experimental spectra. This suggests that at least there is a broad distribution in the thickness in making the inner transition-metal nanoshell. However, the theoretical results also suggest that the scattering yield in Figure 2B is only a fraction of the absorption yield for both of the double-shell nanocages. This encouraged us to carry out the modulation experiment, where the time-dependent amplitude depends on the amount of light absorbed (which is rapidly converted into heat).

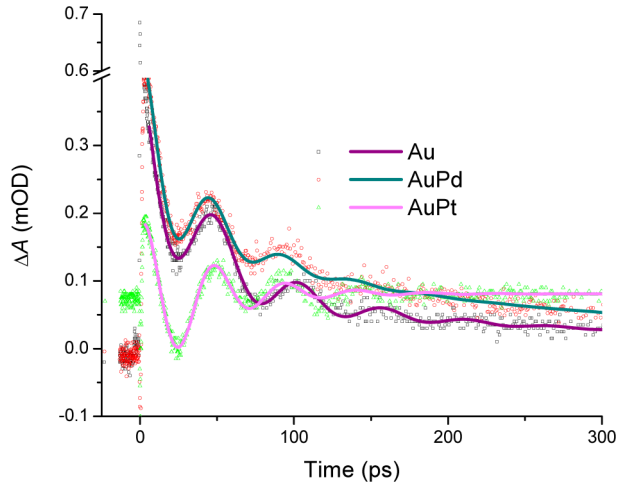

Figure 3. TA dynamics for aqueous solutions of Au and bimetallic nanocages, excited at incident pump fluences of 8.4 and 25 μJ/cm^2 for Au and bimetallic particles, respectively. The transients shown were acquired at probe wavelengths of 794.8 nm for AuNCs, 744.3 nm for AuPdNCs, and 785.2 nm for AuPtNCs. The solid lines represent fits of each data set to the sum of up to two exponential decays and a damped oscillator, ignoring the transient spike near time zero (see the text for additional details).

Effect of the Stiff Transition-Metal Nanoshell on the Breathing Lattice Vibrational Frequency of the Soft Gold Nanoshell. Figure 3 shows TA signals at representative wavelengths for aqueous solutions of the nanocages. The AuNC dynamics are well-described by a single oscillation frequency (eq 1) at all probe wavelengths, with data resembling that published by Hartland's group.[30,31] The dynamics of AuPdNCs and AuPtNCs look qualitatively similar. Damped oscillations are also obtained if the nanocages are measured as a Langmuir–Blodgett monolayer, but the dynamical behavior is changed (see Table 1 and the discussion below). Dynamics at additional probe wavelengths are shown in the Supporting Information.

Fourier transform power spectra of the data (Figure S1, Supporting Information) show broad distributions near 20 GHz, in agreement with the values found through fitting the time domain data (Table 1). The widths of the distributions are likely due to inhomogeneity in the ensembles; the data are averaged over many, randomly oriented nanoparticles. A higher-frequency mode at ~50 GHz is suggested in the case of AuPtNCs, but this could not be clearly resolved through fitting data acquired at any of the probe wavelengths.

The greater stiffness of Pd was observed to decrease the oscillation period (increased the frequency) of the extensional mode of the Au–Pd core–shell nanorods.[32] We believe that the greater stiffness of both Pd and Pt compared with that of Au plays a similar role in the double-shell nanocage structure. It is clear that when platinum is placed inside of the gold nanoshell, the oscillation frequency of the gold shell is higher than that when the interior shell is made of palladium (Table 1). This is consistent with the fact that the Young's modulus value of a

dx.doi.org/10.1021/jz301503z | J. Phys. Chem. Lett. 2012, 3, 3527–3531

platinum thin nanofilm has an elastic constant of 139 GPa while that of palladium is 115 GPa, compared to only 69 GPa for Au.[45] Additionally, our previous work showed the formation of an alloy at the interface between the two metals, which we expect should further stiffen the mechanical response of the Au nanoshell during the symmetric breathing vibration of the cage.[21,43,44]

For a given pump fluence, bimetallic nanocages give weaker TA signals than pure AuNCs. The reduced overall signal for the bimetallic nanoparticles is contrary to their greater extinction value at 400 nm (Figure 2). Because of the double-shell nanoparticle structure, both metals are capable of being excited by the excitation laser. This strongly suggests that, under the conditions of the experiment, either the bimetallic nanocages absorb the pump laser at 400 nm less light than the pure gold nanoshell (which is opposite to what is calculated and shown in Figure 2) or else the absorbed energy in the gold shell is efficiently transferred to the transition-metal lattice vibrations in the double-shell nanocages. The latter could indeed be a possible reason to explain the observation. In Table 1, the lattice vibrational relaxation time, τ_1, is observed to decrease as the transition metal is added to the gold nanocage nanoparticle.

Table 1. Fit of Nanoparticle TA Data to a Damped Oscillator Model[a]

nanoparticles	f_1 (GHz)	φ_1/π	τ_1 (ps)
AuNCs (aq)	17.7 (0.68)	0.188 (0.078)	62 (3.6)
AuPdNCs (aq)	19.1 (1.2)	0.051 (0.038)	51 (3.5)
AuPtNCs (aq)	21.7 (0.11)	1.888 (0.018)	46 (3.8)
AuNCs/quartz	19.0 (0.98)	0.970 (0.045)	38 (1.3)
AuPdNCs/quartz	24.5 (0.92)	0.867 (0.154)	35 (4.8)
AuPtNCs/quartz	22.1 (0.41)	0.984 (0.106)	59 (11)
AgNCs/quartz	36.4 (0.09)	0.083 (0.071)	57 (8.3)

[a]The coherent lattice oscillation frequencies (f_1), phases of signal components (φ_1), and the lattice vibration relaxation times (τ_1) of hollow AuNCs, AuPdNCs, and AuPtNCs and of solid AgNCs in aqueous solutions and on the surface of quartz or glass substrates are given. The effects of the solvent, substrate, and type of the nanoparticle (solid or hollow) on the coherent lattice oscillation frequency are clearly shown. Values shown are the average of results at multiple probe wavelengths near the LSPR maximum for each sample. In parentheses, the standard deviation of the results at multiple wavelengths near the LSPR maximum is given.

Substrate Effect on the Nanocage Oscillation Frequencies. Table 1 compares the values of the gold shell oscillation frequencies of the three cages when dissolved in an aqueous medium with those when placed on solid quartz substrates. The smallest frequency change occurs for the stiffest nanoparticles, the AuPtNCs, an increase of only 2 ± 2% (based on ±1 standard deviation) when going from aqueous solution to a substrate. The softest particles, the AuNCs, and the intermediate AuPdNCs show similar increases upon being moved to a substrate, 10 ± 10% for AuNCs and 30 ± 10% for AuPdNCs. It should be noted that the AuPdNCs show the greatest variability between measurements and from wavelength to wavelength, which is reflected in the standard deviations in Table 1. This suggests a greater degree of heterogeneity in this material compared to that for the other nanocages. The reason for this difference remains a question for further study. A possible explanation lies in the greater miscibility of the Au−Pd system compared to the Au−Pt system,[46] which could result in greater variability in the inner shell thickness.

Coherent Lattice Oscillations of Hollow versus Solid Nanocubes. Table 1 also compares the lattice oscillation frequency of the gold nanocage (17.7 GHz) and solid silver nanocube (36.4 GHz). Both silver and gold have comparable elastic constants; thus, the 50% increase in the oscillation frequency of the silver nanocube (compared with the gold nanocage) must result from the fact that it is a solid nanoparticle, while the gold nanocage is hollow. This conclusion can also be made from the results of the Hartland group.[31] In Figure 4 of their paper, the nanocage vibrational frequency at fixed wall length is found to increase as the wall thickness increases (i.e., as the nanocage fills up). This suggests that the mechanical stability of the nanocage increases as its wall thickness increases.

Depending on the desired size selectivity for catalysis or chemical sensing, the interior dimensions of hollow nanoparticles should be chosen carefully to optimize their durability. The great flexibility with which mechanical properties may be tuned on the nanoscale by simple changes in chemical composition and/or environment could prove relevant for a wide range of applications.

■ ASSOCIATED CONTENT

Supporting Information

Fourier transform of the TA of the hollow nanoparticles (Figure S1). The TA dynamics spectrum of Au, Au−Pd, and Au−Pt nanoparticles pumped at 400 nm and probed at different wavelengths (Figures S2−S4). This material is available free of charge via the Internet at http://pubs.acs.org.

■ AUTHOR INFORMATION

Corresponding Author

*E-mail: melsayed@gatech.edu.

Notes

The authors declare no competing financial interest.

■ ACKNOWLEDGMENTS

This work was supported by the NSF grant (0957335).

■ REFERENCES

(1) Malinsky, M. D.; Kelly, K. L.; Schatz, G. C.; Van Duyne, R. P. Nanosphere Lithography: Effect of Substrate on the Localized Surface Plasmon Resonance Spectrum of Silver Nanoparticles. *J. Phys. Chem. B* **2001**, *105*, 2343−2350.

(2) Kreibig, U.; Vollmer, M. *Optical Properties of Metal Clusters*; Springer Series in Materials Science 25; Springer: New York, 1995

(3) Link, S.; El-Sayed, M. A. Shape and Size Dependence of Radiative, Non-radiative and Photothermal Properties of Gold Nanocrystals. *Int. Rev. Phys. Chem.* **2000**, *19*, 409−453.

(4) Solis, D.; Willingham, B.; Nauert, S. L.; Slaughter, L. S.; Olson, J.; Swanglap, P.; Paul, A.; Chang, W. S.; Link, S. Electromagnetic Energy Transport in Nanoparticle Chains via Dark Plasmon Modes. *Nano Lett.* **2012**, *12*, 1349−1353.

(5) Jin, Y. D.; Jia, C. X.; Huang, S. W.; O'Donnell, M.; Gao, X. H. Multifunctional Nanoparticles as Coupled Contrast Agents. *Nat. Commun.* **2010**, *1*, 41.

(6) Darugar, Q.; Qian, W.; El-Sayed, M. A.; Pileni, M. P. Size-Dependent Ultrafast Electronic Energy Relaxation and Enhanced Fluorescence of Copper Nanoparticles. *J. Phys. Chem. B* **2006**, *110*, 143−149.

(7) Sun, Y. G.; Xia, Y. N. Shape-Controlled Synthesis of Gold and Silver Nanoparticles. *Science* **2002**, *298*, 2176−2179.

(8) Mahmoud, M. A.; El-Sayed, M. A. Comparative Study of the Assemblies and the Resulting Plasmon Fields of Langmuir−Blodgett Assembled Monolayers of Silver Nanocubes and Gold Nanocages. *J. Phys. Chem. C* **2008**, *112*, 14618−14625.
(9) Petrova, H.; Lin, C.-H.; de Liejer, S.; Hu, M.; McLellan, J. M.; Siekkinen, A. R.; Wiley, B. J.; Marquez, M.; Xia, Y.; Sader, J. E.; Hartland, G. V. Time-Resolved Spectroscopy of Silver Nanocubes: Observation and Assignment of Coherently Excited Vibrational Modes. *J. Chem. Phys.* **2007**, *126*, 094709−094716.
(10) Jana, N. R.; Gearheart, L.; Murphy, C. J. Wet Chemical Synthesis of High Aspect Ratio Cylindrical Gold Nanorods. *J. Phys. Chem. B* **2001**, *105*, 4065−4067.
(11) Nikoobakht, B.; El-Sayed, M. A. Preparation and Growth Mechanism of Gold Nanorods (NRs) Using Seed-Mediated Growth Method. *Chem. Mater.* **2003**, *15*, 1957−1962.
(12) Nehl, C. L.; Liao, H. W.; Hafner, J. H. Optical Properties of Star-Shaped Gold Nanoparticles. *Nano Lett.* **2006**, *6*, 683−688.
(13) Jin, R.; Cao, Y. C.; Hao, E.; Metraux, G. S.; Schatz, G. C.; Mirkin, C. A. Controlling Anisotropic Nanoparticle Growth Through Plasmon Excitation. *Nature (London, U.K.)* **2003**, *425*, 487−490.
(14) Oldenburg, S. J.; Averitt, R. D.; Westcott, S. L.; Halas, N. J. Nanoengineering of Optical Resonances. *Chem. Phys. Lett.* **1998**, *288*, 243−247.
(15) Kelf, T. A.; Tanaka, Y.; Matsuda, O.; Larsson, E. M.; Sutherland, D. S.; Wright, O. B. Ultrafast Vibrations of Gold Nanorings. *Nano Lett.* **2011**, *11*, 3893−3898.
(16) Mahmoud, M. A.; Snyder, B.; El-Sayed, M. A. Surface Plasmon Fields and Coupling in the Hollow Gold Nanoparticles and Surface-Enhanced Raman Spectroscopy. Theory and Experiment. *J. Phys. Chem. C* **2010**, *114*, 7436−7443.
(17) Mahmoud, M. A.; El-Sayed, M. A. Aggregation of Gold Nanoframes Reduces, Rather Than Enhances, SERS Efficiency Due to the Trade-Off of the Inter- and Intraparticle Plasmonic Fields. *Nano Lett.* **2009**, *9*, 3025−3031.
(18) Mahmoud, M. A.; El-Sayed, M. A. Gold Nanoframes: Very High Surface Plasmon Fields and Excellent Near-Infrared Sensors. *J. Am. Chem. Soc.* **2010**, *132*, 12704−12710.
(19) Hodak, J. H.; Henglein, A.; Hartland, G. V. Tuning the Spectral and Temporal Response in PtAu Core−Shell Nanoparticles. *J. Chem. Phys.* **2001**, *114*, 2760−2765.
(20) Zeng, J.; Zhang, Q.; Chen, J. Y.; Xia, Y. N. A Comparison Study of the Catalytic Properties of Au-Based Nanocages, Nanoboxes, and Nanoparticles. *Nano Lett.* **2010**, *10*, 30−35.
(21) Mahmoud, M. A.; Saira, F.; El-Sayed, M. A. Experimental Evidence For The Nanocage Effect In Catalysis With Hollow Nanoparticles. *Nano Lett.* **2010**, *10*, 3764−3769.
(22) Juve, V.; Scardamaglia, M.; Maioli, P.; Crut, A.; Merabia, S.; Joly, L.; Del Fatti, N.; Vallee, F. Cooling Dynamics and Thermal Interface Resistance of Glass-Embedded Metal Nanoparticles. *Phys. Rev. B* **2009**, *80*, 195406−195411.
(23) Bonacina, L.; Callegari, A.; Bonati, C.; van Mourik, F.; Chergui, M. Time-Resolved Photodynamics of Triangular-Shaped Silver Nanoplates. *Nano Lett.* **2006**, *6*, 7−10.
(24) Del Fatti, N.; Voisin, C.; Chevy, F.; Vallee, F.; Flytzanis, C. Coherent Acoustic Mode Oscillation and Damping in Silver Nanoparticles. *J. Chem. Phys.* **1999**, *110*, 11484−11487.
(25) Hodak, J. H.; Martini, I. Observation of Acoustic Quantum Beats in Nanometer Sized Au Particles. *J. Chem. Phys.* **1998**, *108*, 9210−9213.
(26) Hartland, G. V. Optical Studies of Dynamics in Noble Metal Nanostructures. *Chem. Rev.* **2011**, *111*, 3858−3887.
(27) Huang, W.; Qian, W.; El-Sayed, M. A. Coherent Vibrational Oscillation in Gold Prismatic Monolayer Periodic Nanoparticle Arrays. *Nano Lett.* **2004**, *4*, 1741−1747.
(28) Huang, W.; Qian, W.; El-Sayed, M. A. The Optically Detected Coherent Lattice Oscillations in Silver and Gold Monolayer Periodic Nanoprism Arrays: The Effect of Interparticle Coupling. *J. Phys. Chem. B* **2005**, *109*, 18881−18888.
(29) Huang, W.; Qian, W.; Jain, P. K.; El-Sayed, M. A. The Effect of Plasmon Field on the Coherent Lattice Phonon Oscillation in Electron-Beam Fabricated Gold Nanoparticle Pairs. *Nano Lett.* **2007**, *7*, 3227−3234.
(30) Hu, M.; Petrova, H.; Chen, J.; McLellan, J. M.; Siekkinen, A. R.; Marquez, M.; Li, X.; Xia, Y.; Hartland, G. V. Ultrafast Laser Studies of the Photothermal Properties of Gold Nanocages. *J. Phys. Chem. B* **2006**, *110*, 1520−1524.
(31) Petrova, H.; Lin, C.-H.; Hu, M.; Chen, J.; Siekkinen, A. R.; Xia, Y.; Sader, J. E.; Hartland, G. V. Vibrational Response of Au−Ag Nanoboxes and Nanocages to Ultrafast Laser-Induced Heating. *Nano Lett.* **2007**, *7*, 1059−1063.
(32) Cardinal, M. F.; Mongin, D.; Crut, A.; Maioli, P.; Rodríguez-González, B.; Pérez-Juste, J.; Liz-Marzán, L. M.; Del Fatti, N.; Vallée, F. Acoustic Vibrations in Bimetallic Au@Pd Core−Shell Nanorods. *J. Phys. Chem. Lett.* **2012**, *3*, 613−619.
(33) Hu, M.; Wang, X.; Hartland, G. V.; Mulvaney, P.; Juste, J. P.; Sader, J. E. Vibrational Response of Nanorods to Ultrafast Laser Induced Heating: Theoretical and Experimental Analysis. *J. Am. Chem. Soc.* **2003**, *125*, 14925−14933.
(34) Hu, M.; Petrova, H.; Sekkinen, A. R.; Chen, J.; McLellan, J. M.; Li, Z.-Y.; Marquez, M.; Li, X.; Xia, Y.; Hartland, G. V. Optical Properties of Au−Ag Nanoboxes Studied by Single Nanoparticle Spectroscopy. *J. Phys. Chem. B* **2006**, *110*, 19923−19928.
(35) van Dijk, M. A.; Lippitz, M.; Orrit, M. Detection of Acoustic Oscillations of Single Gold Nanospheres by Time-Resolved Interferometry. *Phys. Rev. Lett.* **2005**, *95*, 267406−267410.
(36) Staleva, H.; Hartland, G. V. Transient Absorption Studies of Single Silver Nanocubes. *J. Phys. Chem. C* **2008**, *112*, 7535−7539.
(37) Staleva, H.; Hartland, G. V. Vibrational Dynamics of Silver Nanocubes and Nanowires Studied by Single-Particle Transient Absorption Spectroscopy. *Adv. Funct. Mater* **2008**, *18*, 3809−3817.
(38) Hartland, G. V. Ultrafast Studies of Single Semiconductor and Metal Nanostructures Through Transient Absorption Microscopy. *Chem. Sci.* **2010**, *1*, 303−309.
(39) Muskens, O. L.; Del Fatti, N.; Vallée, F. Femtosecond Response of a Single Metal Nanoparticle. *Nano Lett.* **2006**, *6*, 552−556.
(40) Voisin, C.; Del Fatti, N.; Christofilos, D.; Vallée, F. Ultrafast Electron Dynamics and Optical Nonlinearities in Metal Nanoparticles. *J. Phys. Chem. B* **2001**, *105*, 2264−2280.
(41) Hodak, J. H.; Henglein, A.; Hartland, G. V. Coherent Excitation of Acoustic Breathing Modes in Bimetallic Core−Shell Nanoparticles. *J. Phys. Chem. B* **2000**, *104*, 5053−5055.
(42) Pelton, M.; Sader, J. E.; Burgin, J.; Liu, M.; Guyot-Sionnest, P.; Gosztola, D. Damping of Acoustic Vibrations in Gold Nanoparticles. *Nat. Nano* **2009**, *4*, 492−495.
(43) Mahmoud, M. A.; El-Sayed, M. A. Metallic Double Shell Nanocages: The Challenges of Their Synthetic Techniques. *Langmuir* **2012**, *28*, 4051−4059.
(44) Mahmoud, M. A.; El-Sayed, M. A. Time Dependence and Signs of the Shift of the Surface Plasmon Resonance Frequency in Nanocages Elucidate the Nanocatalysis Mechanism in Hollow Nanoparticles. *Nano Lett.* **2011**, *11*, 946−953.
(45) Vaz, A. R.; Salvadori, M. C.; Cattani, M. Young Modulus Measurement of Nanostructured Metallic Thin Films. *J. Metastable Nanocryst. Mater.* **2004**, *20*−*21*, 758−762.
(46) Bond, G. C. The Electronic Structure of Platinum−Gold Alloy Particles. *Platinum Met. Rev.* **2007**, *51*, 63−68.